

## Effect of gain saturation on the nonlinear dynamical behavior of optically injected semiconductor lasers

Furat Ahmad AL-SAYMARI, Imad Al-Deen Hussein AL-SAIDI\*,  
May Jassim ASHOOR

Department of Physics, College of Education for Pure Sciences, University of Basrah, Basrah, Iraq

Received: 24.12.2012 • Accepted: 27.08.2013 • Published Online: 17.01.2014 • Printed: 14.02.2014

**Abstract:** We studied numerically the dynamics and bifurcations route to chaos of an optically injected semiconductor laser. The sequence of bifurcations mainly followed the period-doubling scenario. Observations of different kinds of injected semiconductor laser dynamical behaviors including stable state, periodic oscillation state, quasi-periodic oscillation state, co-existence of periodic and chaotic states, and period-3 and period-6 oscillation states are reported.

The existence of isolated branches created from a sudden jump in the dynamics of the semiconductor laser was also observed in the bifurcation diagram. In order to draw a detailed picture for the dynamical behavior of the semiconductor laser, we constructed color stability maps describing the laser system dynamics as a function of the pumping current ( $P$ ) and the injection field strength ( $\eta$ ) for 2 cases, without and with gain saturation effect.

**Key words:** Nonlinear dynamics, bifurcations, period-doubling, chaos, semiconductor lasers

### 1. Introduction

The semiconductor laser with external optical injection is one of the best candidates for studying nonlinear dynamic phenomena in optics. This laser has been shown (both theoretically and experimentally) to induce various interesting nonlinear dynamical behaviors in laser output due to the influence of the laser operating parameters. These include steady-state oscillations, period-doubling bifurcations, quasi-periodic oscillations, co-existence of dynamical behaviors with multiple attractors, and chaos [1–5].

The semiconductor laser with optical injection and optical feedback has received considerable attention due to its possible applications in many different areas, such as for all-optical switching data [6], encoding and decoding information [7,8], photonic microwave generation and transmission [9], and private and secure optical communication systems using synchronization [3,8,10–12].

The chaos in the semiconductor laser with optical injection or optical feedback can be controlled and stabilized into stable oscillations simply by varying the laser control parameters. The stabilization of the output intensity in such a laser system is of great concern in many applications [3,13,14].

In spite of the existence of a number of investigations (experimental and theoretical) on the semiconductor laser, the study of the dynamical behaviors of this laser system has still received great attention in order to explore and understand the complicated dynamics of this system. In this paper we report a detailed study and analysis of the nonlinear dynamics of a single-mode optically injected semiconductor laser. Our study was based on a simple model of rate equations.

\*Correspondence: [al\\_saidi\\_imad@yahoo.com](mailto:al_saidi_imad@yahoo.com)

## 2. Theory

For our study, we consider a single-mode semiconductor laser subjected to an external optical injection governed by the following modified Lang–Kobayashi dimensionless rate equations for the complex electric field ( $E$ ) and the carrier density ( $N$ ) [15–17]:

$$\dot{E} = (1 - ib)GE + \eta e^{-i\Delta t} \quad (1)$$

$$T\dot{N} = P - N - P(1 + 2G)|E|^2, \quad (2)$$

where  $b$  is the line-width enhancement factor, coupling the gain variations to the refraction index of the laser medium;  $\eta$  is the injection field strength;  $\Delta$  is the optical frequency detuning between the injecting laser and the injected laser;  $T$  is the ratio of the carrier and photon lifetimes;  $P$  is the pumping current above the threshold; and  $G$  is the nonlinear gain, defined by

$$G = N - \varepsilon P(|E|^2 - 1) \quad (3)$$

where  $\varepsilon$  is the gain saturation coefficient (parameter).

In order to extend our study of the dynamical behavior of an injected semiconductor laser, we include in the rate equations the phase difference between the injection field and the injected laser ( $\varphi$ ). This can be achieved by introducing a basic solution of the form  $E = Ae^{i(\varphi - \Delta t)}$  into Eqs. (1)–(3) and solving for  $A$ ,  $\varphi$ , and  $N$ . This leads to the following relations:

$$dA/dt = G'A + \eta \cos\varphi \quad (4)$$

$$d\varphi/dt = \Delta - bG' - (\eta/A)\sin\varphi, \quad (5)$$

and

$$T(dN/dt) = P - N - P[1 + 2G']A^2, \quad (6)$$

where

$$G' = N - \varepsilon P(A^2 - 1). \quad (7)$$

$A$  represents the electric field amplitude of the injected laser.

To find the steady-state points of the laser dynamic variables, we substitute the following steady-state solutions,  $dA/dt = 0$ ,  $d\varphi/dt = 0$ ,  $dN/dt = 0$ , and  $A = A_S$ ,  $\varphi = \varphi_S$ ,  $N = N_S$  into Eqs. (4)–(6) and then we solve the resulting equations for the case of zero detuning ( $\Delta = 0$ ) and negligible gain saturation effect ( $\varepsilon = 0$ ). This leads to the following reduced equations:

$$\varphi_S = \tan^{-1}(b) \quad (8)$$

and

$$\eta^2 = A_S^2 N_S^2 (1 + b^2) \quad (9)$$

From Eq. (6), we have

$$A_S^2 = \frac{P - N_S}{P(1 + 2N_S)} \quad (10)$$

By substituting Eq. (10) into Eq. (9), we obtain the following relation:

$$N_S^3(1 + b^2) - PN_S^2(1 + b^2) + 2P\eta^2 N_S + P\eta^2 = 0 \quad (11)$$

The locations of the stationary points (or the Hopf bifurcation points) can be determined from the derivation of Eq. (11), and then solving for  $N_S$  will lead to the following relationships:

$$3N_S^2(1 + b^2) - 2PN_S(1 + b^2) + 2P\eta^2 = 0 \quad (12)$$

and

$$N_S = \frac{P(1 + b^2) \pm [P^2(1 + b^2)^2 - 6P\eta^2(1 + b^2)]^{1/2}}{3(1 + b^2)} \quad (13)$$

This bifurcation point defines the region of laser locking where the laser produces output with constant intensity at the frequency of the injected light. The branch of the periodic solution emerges from this Hopf bifurcation point.

It is seen in Eq. (13) that the bifurcation point depends on the main laser control parameters; varying any one of these parameters causes a change in the locations of the Hopf bifurcation point, and this may lead to modification in the laser dynamical behaviors.

### 3. Results and discussion

Figures 1a–1k show the numerically calculated bifurcation diagrams from Eqs. (1)–(3) by using the fourth-order Runge–Kutta algorithm with the help of a Fortran 90 program. The maxima of the laser intensity ( $I_{\max}$ ) as a function of the injection field strength ( $\eta$ ) are plotted for different representative values of pumping current ( $P$ ), over the range  $P = 0.1$ – $1.0$ . The values of the other laser operating parameters are fixed at  $b = 3.2$ ,  $T = 165$ ,  $\Delta = 0$  (zero detuning frequency), and  $\varepsilon = 0$  (for the case of the absence of gain saturation effect). For more clarity, we have extended the scale of the  $\eta$ -values. It is clearly seen in this figure that the chaotic dynamical behavior is dominant with some regions of period-doubling and reverse period-doubling sequences' route to chaos shown on both sides of the chaotic region. These represent period-one (P1) oscillation state evolving into period-two (P2) oscillation state, and finally reaching chaotic oscillation state with an increase in the value of  $P$ . Narrow regions of periodic states within the broadened chaotic region are also seen in this diagram.

With increasing value of the pumping current parameter ( $P$ ), the region of the chaotic emission behavior progressively shifts towards higher values of the field injection strength ( $\eta$ ). This results in increasing of the interval of the P1 oscillation state region until the appearance of the whole region at  $P = 0.56$  (Figure 1f). Then when the value of  $P$  increases to 0.62 the Hopf bifurcation point starts to appear (the blue circular dot), as shown in Figure 1g. It is progressively shifted towards bigger  $\eta$ -values as the value of  $P$  increases, and, consequently, the domain of the steady-state output region is extended further.

In order to examine the dynamical behavior of the semiconductor laser system when the effect of gain saturation is taken into account ( $\varepsilon \neq 0$ ), we set  $\varepsilon$  to a certain value of 0.011, keeping the other laser parameters as in Figure 1. Then we start to increase the value of  $P$  over the same range in Figure 1; the obtained numerical results are shown in Figure 2. The laser dynamical behavior in this case is completely different from that in Figure 1. The dynamical behavior here begins from the chaotic regime over a certain range of  $P$ -values. The chaotic regime progressively decreases with increasing value of  $P$  and some of branches of periodic oscillations

start to appear and become easy to identify, even those embedded in the chaotic region. We identify different co-existing types of behaviors in the bifurcation diagram. They are extended over different ranges of  $\eta$ ; these are: P1 oscillations, P2 oscillations, period-four (P4) oscillations, period-three (P3) oscillations, and period-six (P6) oscillations.

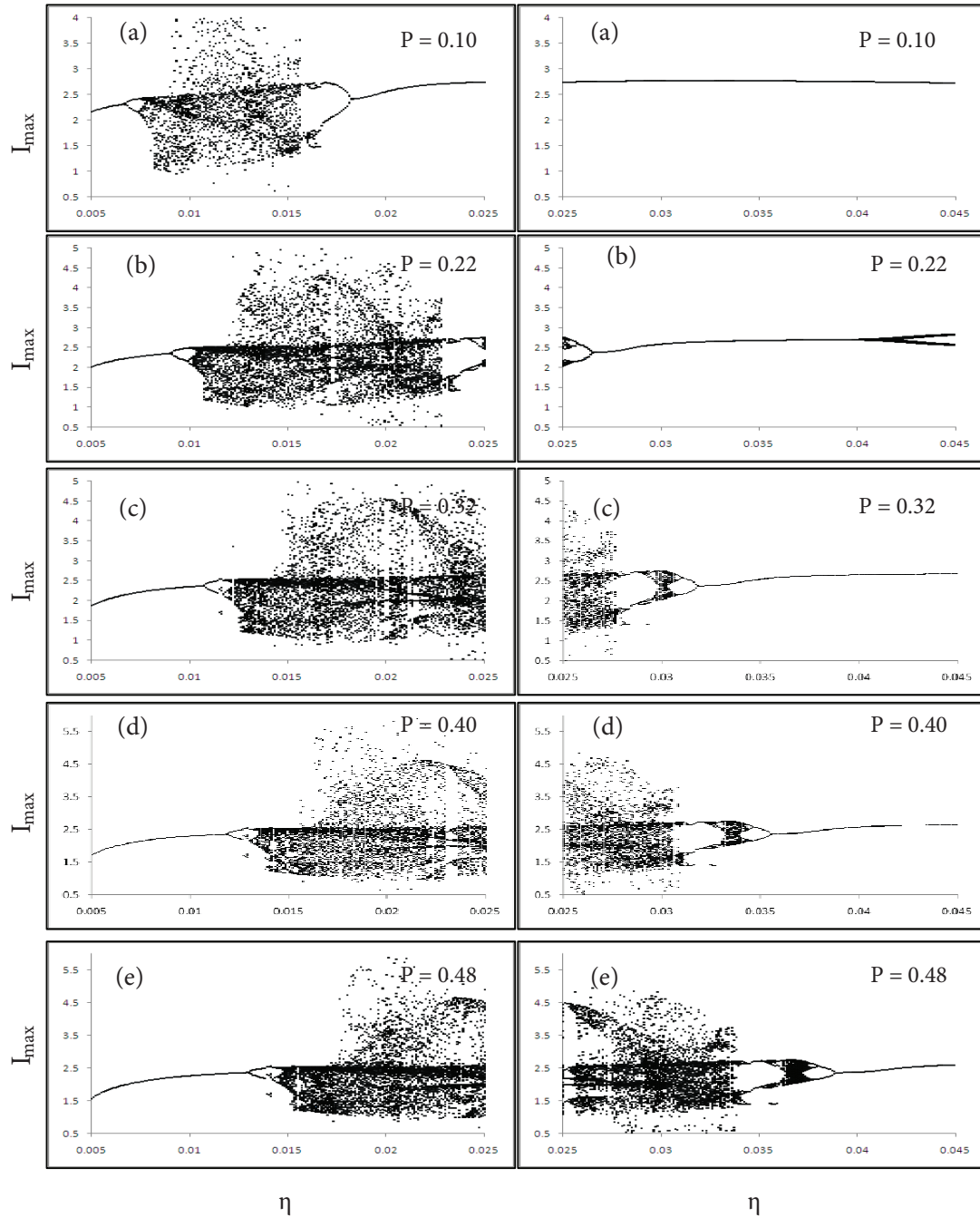


**Figure 1.** Numerically calculated bifurcation diagram. Maximum laser output intensity ( $I_{max}$ ) versus injection field strength ( $\eta$ ) for different pumping current ( $P$ ) with  $\varepsilon = 0$ . The laser parameters values:  $b = 3.2$ ,  $T = 165$ , and  $\Delta = 0$ . The Hopf bifurcation point is shifted toward higher values of  $\eta$  as the value of  $P$  increases.

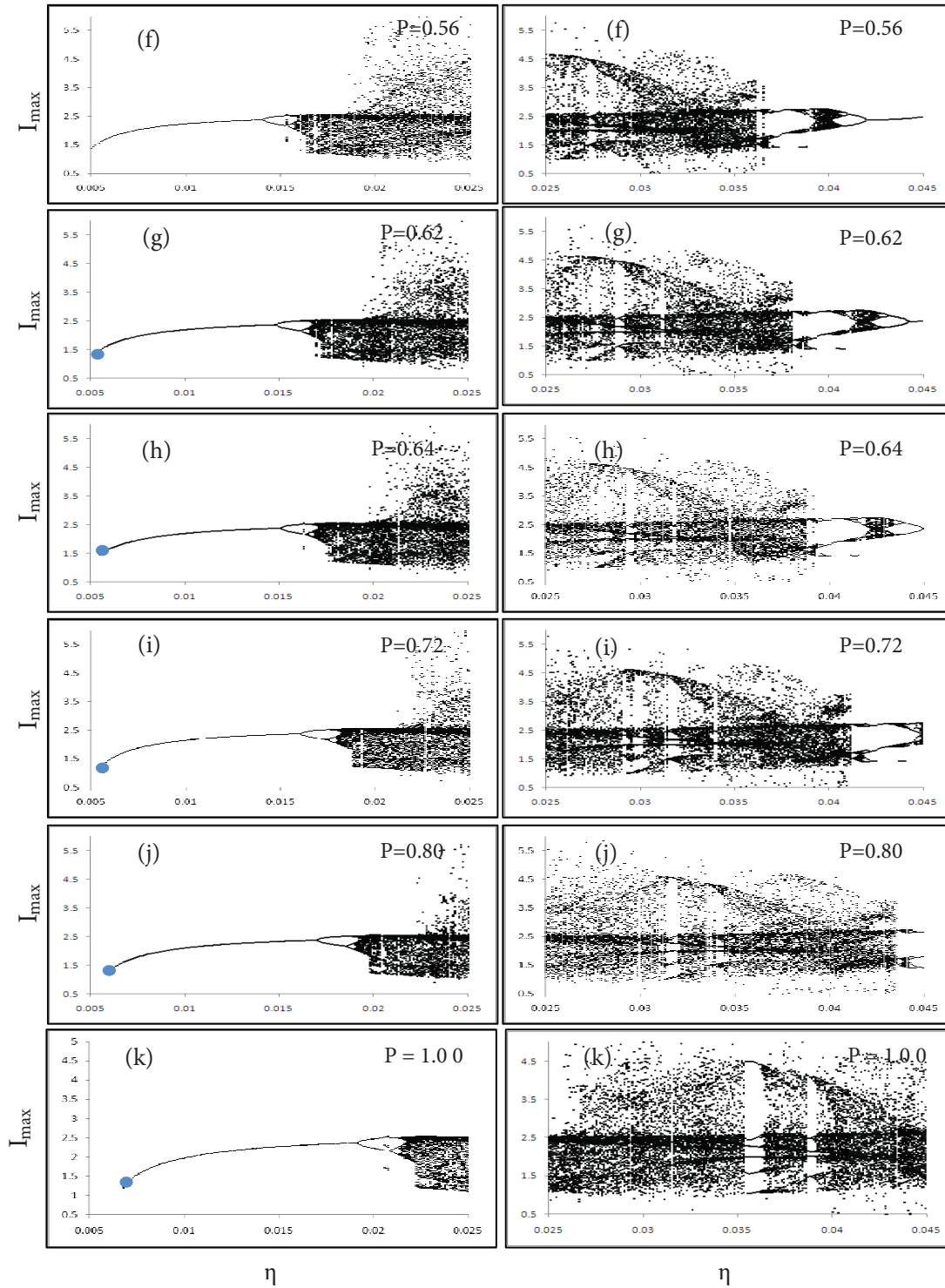
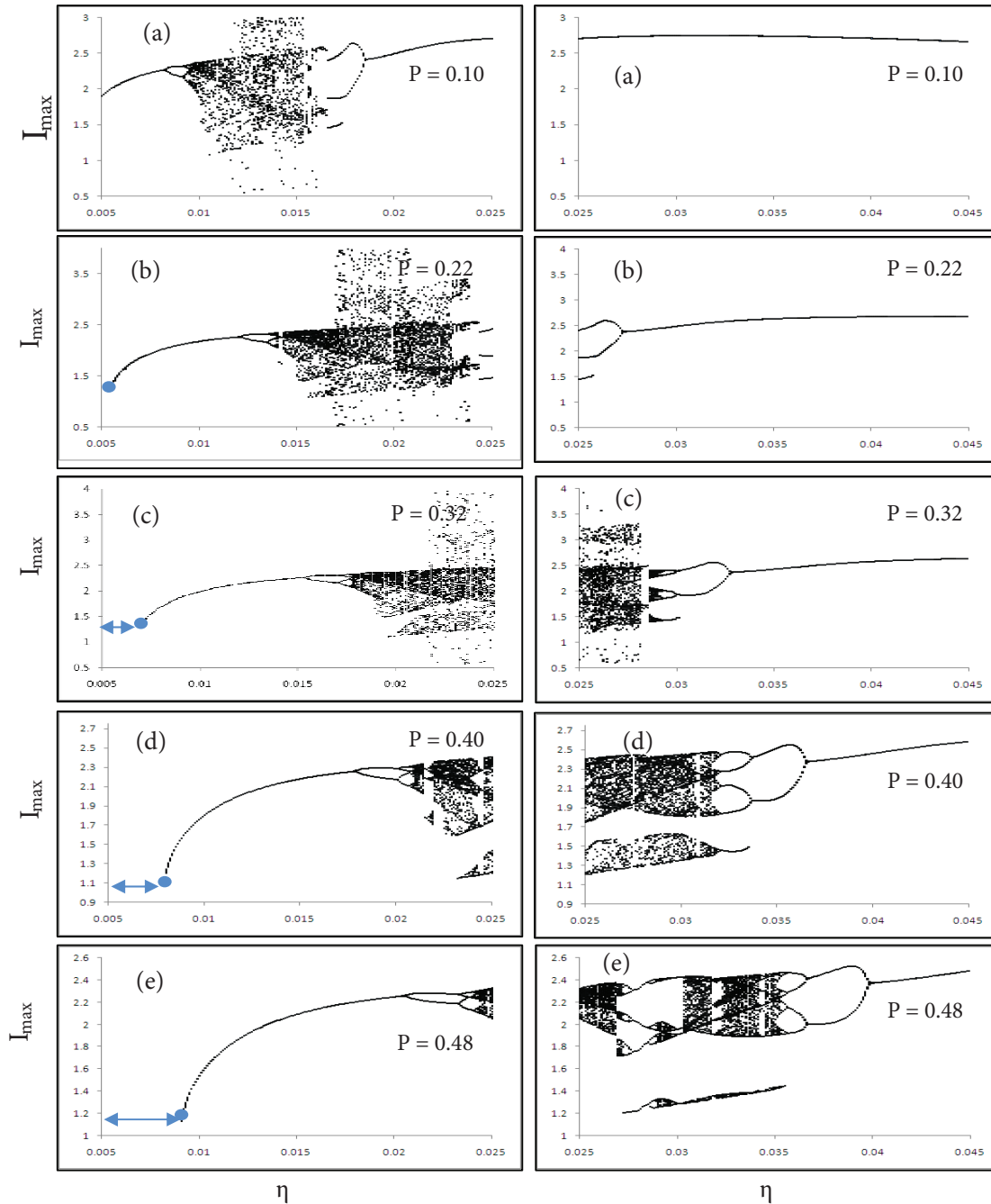


Figure 1. Continued.

As the value of  $P$  keeps increasing, the region of the chaotic regime is reduced and consequently the domain of the periodic oscillation state region is increased and becomes wider. When the value of  $P$  is increased, the chaotic emission behavior entirely disappears and the laser starts to exhibit only P1 and P2 oscillations outputs,

as shown in Figures 2i and 2j for  $P = 0.72$  and  $P = 0.80$ , respectively. This situation changes when the value of  $P$  is increased further to 1.0, where the stable steady-state domain becomes wider and the laser system starts to exhibit output intensity with sustained P1 oscillations. This situation does not change with further increasing values of  $P$ , even with higher values of  $P$ .

Comparing the cases in Figures 1 and 2 (i.e. without and with the gain saturation effect) shows significant differences in the dynamical behavior between the 2 cases. In the second case ( $\varepsilon = 0.011$ ), the Hopf bifurcation



**Figure 2.** Bifurcation diagram with  $\varepsilon = 0.011$ . The same values of the other parameters as in Figure 1.

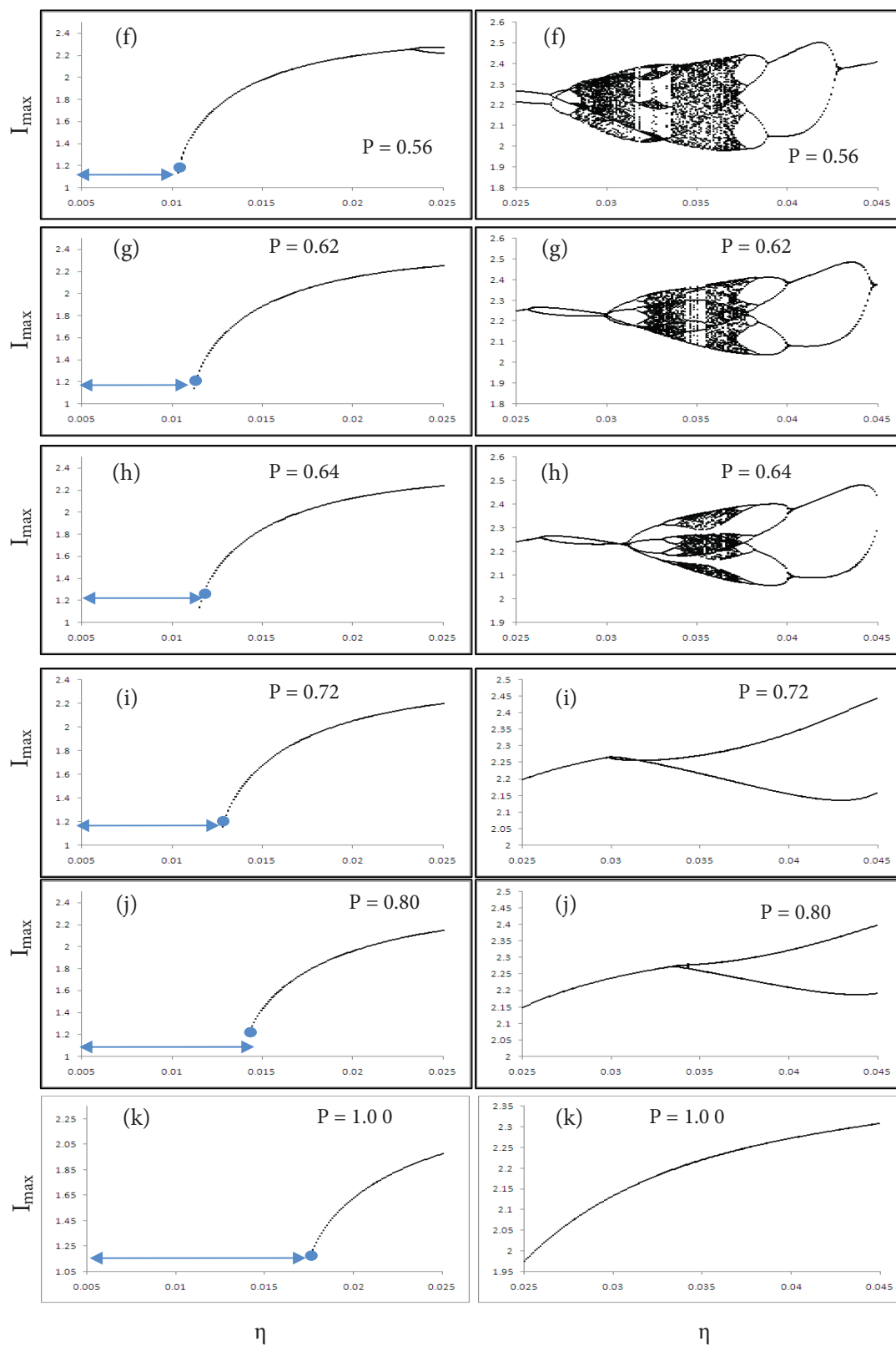


Figure 2. Continued.

point appears earlier (at  $P = 0.22$ ) in comparison with the one in the first case ( $\varepsilon = 0$ ). We note that when the whole branch (the whole  $\eta$ -range) of the P1 oscillation state appears, a further increase in the value of  $P$  does not cause any further extension in this range. Unlike the case of the presence of gain saturation effect ( $\varepsilon \neq 0$ ), as in Figure 2, the ranges of  $\eta$ -value for the stable state and P1 state in the case of neglecting the effect of gain saturation ( $\varepsilon = 0$ ), as in Figure 1, remain extending with increasing values of  $P$ .

A very interesting result can be seen in Figure 2, that is, the sudden appearance of isolated branches (they are not born from the cascade of bifurcations) as the value of  $\eta$  is increased. This is clearly identified in the bifurcation diagrams over the range  $P = 0.10$ – $0.48$ . In contrast to Ref. [17], we note that when  $P = 0.48$ , the bifurcation branch at  $\eta = 0.028$  is a P4 oscillation state in our work, while the bifurcation diagram in Ref. [17] shows a region of P3 oscillation state at this value of  $\eta$ . The difference in the dynamical behaviors in the 2 bifurcation diagrams may be due to the sudden appearance of isolated islands (branches) in our bifurcation diagram, while they are missing in the bifurcation diagram in Ref. [17] for the same value of  $P$ .

In order to extract some additional information concerning the characteristics of the laser dynamical behavior, we have chosen one case from Figure 2, that is, when  $P = 0.48$ , and then we varied the value of  $\eta$  over the range  $\eta = 0.02$ – $0.03$ . We have plotted the time series; the laser output intensity as a function of the time (first column), phase-space portraits; the imaginary part of the electric field  $\text{Im}(E)$  against the real part of the electric field  $\text{Re}(E)$  (second column) and the fast Fourier transformation (FFT) spectra; and the laser intensity as a function of the laser frequency (the third column), for different values of the injection field strength ( $\eta$ ). The results are shown in Figure 3. It is clearly seen that the variation in  $\eta$  causes dramatic changes in the dynamics of the laser system and produces different dynamical behaviors as the value of  $\eta$  is increased. The sequence of transitions of the dynamical behavior starts with P1 state limit cycle at  $\eta = 0.020$  (Figures 3a1, 3b1, and 3c1); followed by P2 state, at  $\eta = 0.021$  (Figures 3a2, 3b2, and 3c2); P4 state, at  $\eta = 0.024$  (Figures 3a3, 3b3, and 3c3); and then the laser system reaches the chaotic state through a quasi-periodic regime, at  $\eta = 0.025$  (Figures 3a4, 3b4, and 3c4).

The phase-space plots display dramatic increases in the orbits of the laser system attractor (Figure 3b4) and the laser system trajectory represents a type of strange attractor [18]. The optical spectrum of the laser output intensity develops to a broad band consisting of a large number of cavity modes that appear to lase simultaneously (Figure 3c4).

When  $\eta$  is increased to 0.028, the chaotic behavior regime disappears and the laser system returns to the periodic behavior regime by revealing P3 oscillations output (Figures 3a5, 3b5, and 3c5) followed by P6 oscillation state at  $\eta = 0.0288$  (Figures 3a6, 3b6, and 3c6), and then returns again to the P3 oscillation state at  $\eta = 0.03$  (Figures 3a7, 3b7, and 3c7). We note that the dynamical behavior states here are consistent with those seen in the bifurcation diagram of Figure 2e, and confirm our numerical calculations.

Next, we will study the effect of laser phase ( $\varphi$ ) on the dynamics of the semiconductor laser. The laser rate equations (4)–(6), in which the laser phase ( $\varphi$ ) is combined with the electric field amplitude ( $A$ ) and the carrier density ( $N$ ), are numerically solved. Figure 4 illustrates, in 3 dimensions (the phase plane diagram), the relation between the laser phase shift ( $\varphi$ ), the electric field amplitude ( $A$ ), and the carrier density ( $N$ ), for different values of  $\eta$ , over the same range of  $\eta$  in Figure 3 (i.e.  $\eta = 0.02$ – $0.03$ ), at fixed values for the other laser operating parameters as in Figure 3. The cases in Figure 4 correspond to those in

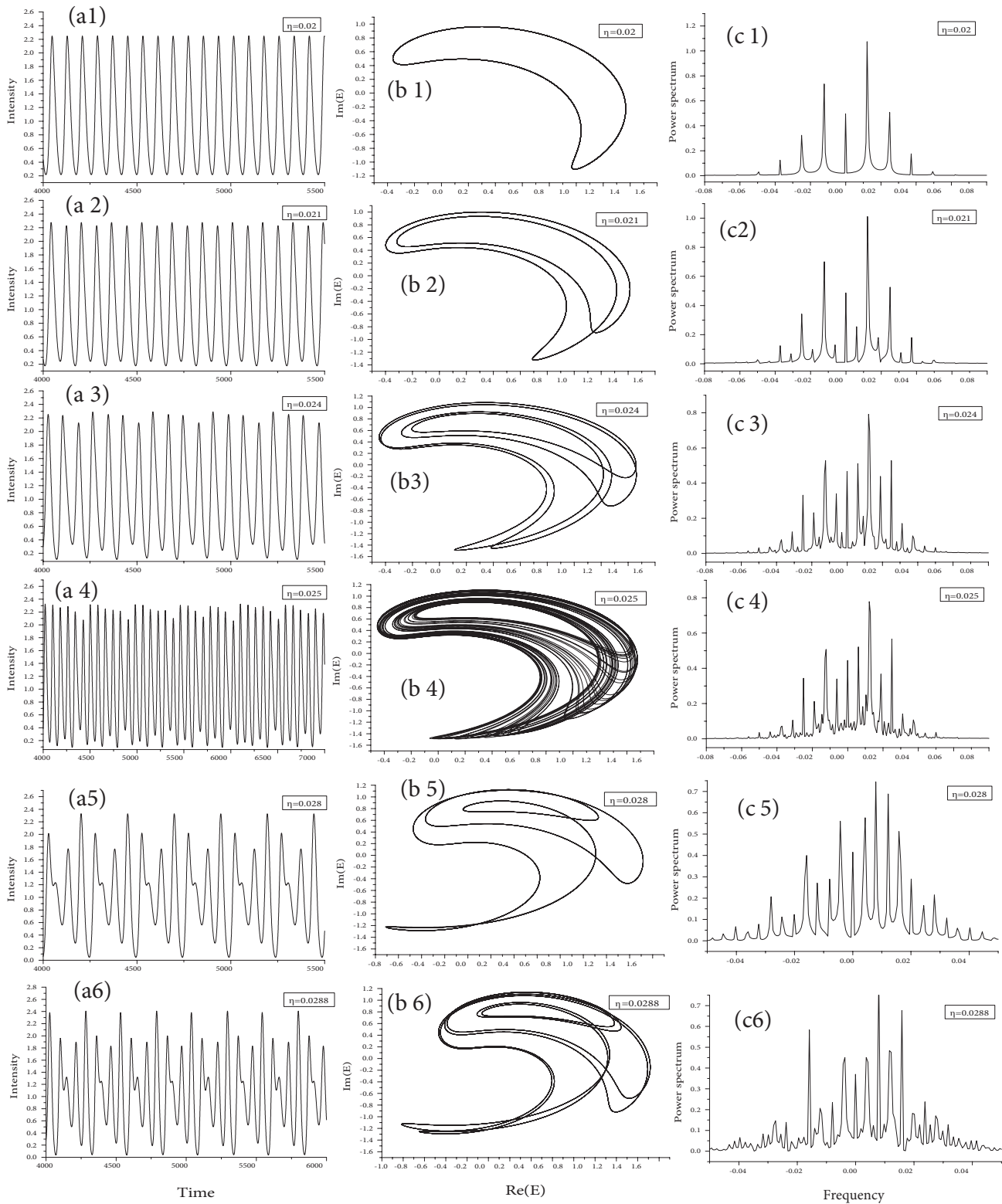


**Figure 3.** Intensity time-series (first column) and the corresponding phase-space portraits (second column) and power spectra (third column) for the case of  $P = 0.48$  in Figure 2, as the value of  $\eta$  increases.

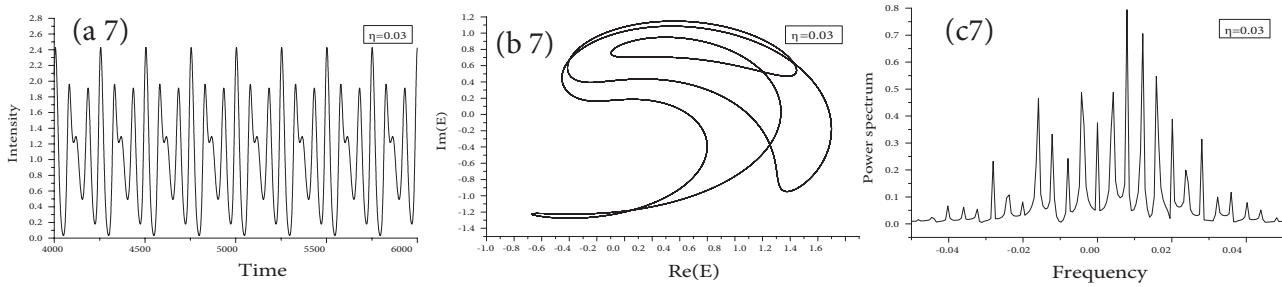


Figure 3. Continued.

Figure 3. The phase-space portrait in Figure 4a is a single limit-cycle trajectory corresponding to P1 oscillation state at  $\eta = 0.020$ , developing to P2 limit-cycles trajectory as the value of  $\eta$  is increased to 0.021 (Figure 4b),

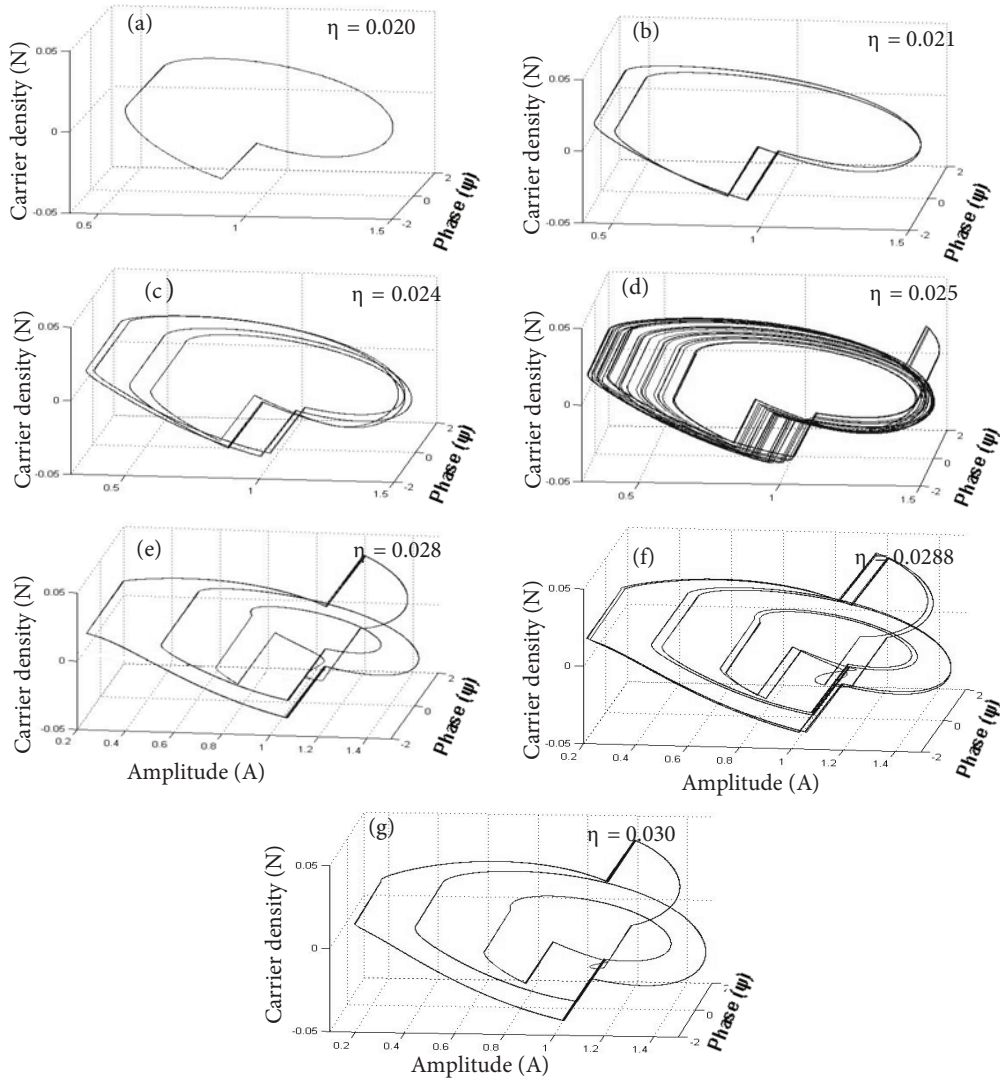
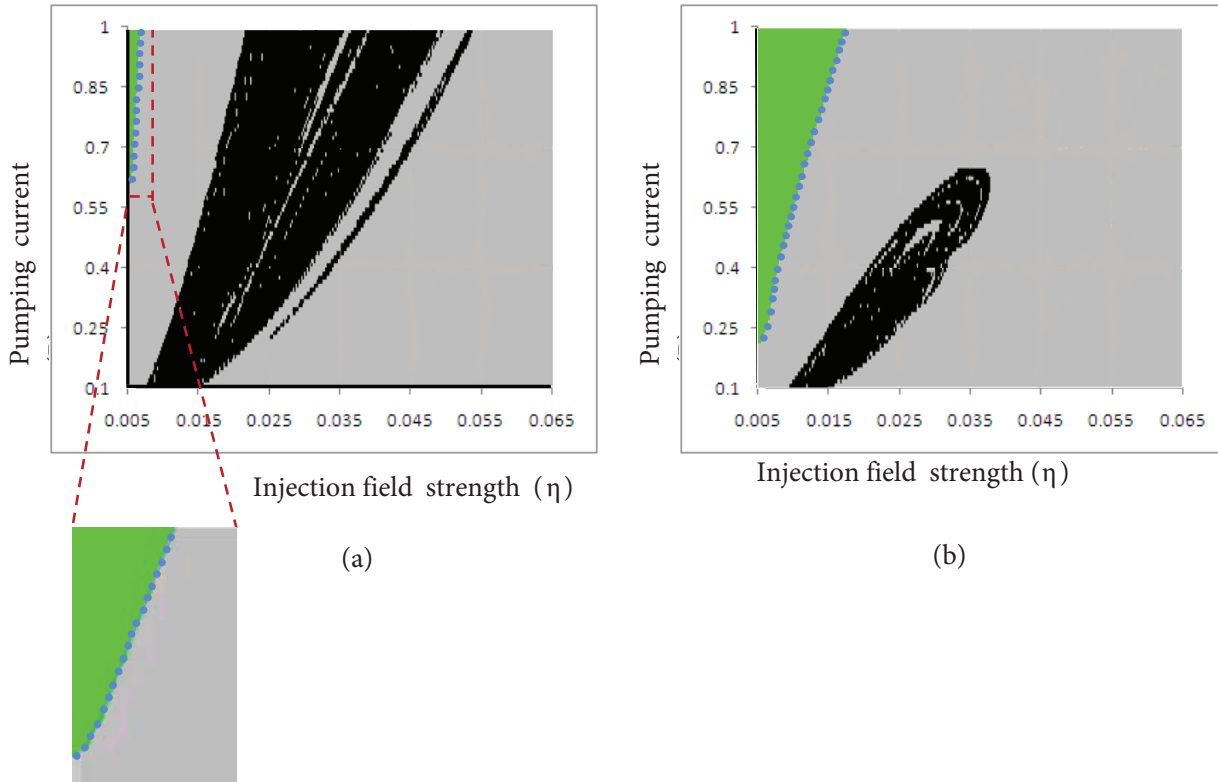


Figure 4. The phase plane diagram as a function of  $A$ ,  $\varphi$ , and  $N$  for different values of  $\eta$ . Different states are indicated: (4a) P1 limit-cycle, (4b) P2, single tours, (4c) P4, (4d) chaotic regime, (4e) P3, (4f) P6, and (4g) P3.

and then to P4 limit-cycles trajectory at  $\eta = 0.024$  (Figure 4c). The laser enters the chaotic regime at  $\eta = 0.025$  (Figure 4d). With increasing values of  $\eta$ , the transition of the attractor trajectory from one bifurcation state to another bifurcation state of different periodic orbits takes place over some certain  $\eta$ -values. These states are: P3 trajectory at  $\eta = 0.028$  (Figure 4e), which switches to P6 trajectory at  $\eta = 0.0288$  (Figure 4f), and then the laser system returns to P3 trajectory at  $\eta = 0.030$  (Figure 4g). It seems that these transitions in the sequence are the most probable transitions for the dynamical behavior of the semiconductor laser system under our particular parameter conditions.

In order to provide an overall picture of the different types of dynamical behavior of an optically injected semiconductor laser system, we have construct 2 detailed color stability maps as a function of the pumping current (P) and injection field strength ( $\eta$ ), which is varied over the range  $\eta = 0.005$ – $0.065$ , as the main laser control parameter, as shown in Figure 5. The 2 maps in this figure belong to 2 cases: one without including the effect of gain saturation ( $\varepsilon = 0$ ) and the other with including this effect ( $\varepsilon = 0.011$ ), as shown in Figures 5a and 5b, respectively. These 2 maps clearly show different regions corresponding to different dynamical behavior states of the laser output intensity. To distinguish between these dynamical behaviors, we use color coding. Each behavior state has a different color. Green stands for stable locking solutions (fixed points), gray for periodic oscillation state, black for chaotic oscillation state, and blue for the Hopf bifurcation points.

By comparing the 2 stability maps in Figures 5a and 5b, we see different behavior structures. When there is no gain saturation (i.e. when the effect of gain saturation is not included in the numerical calculations ( $\varepsilon = 0$ )), the region (the dimension) of the chaotic attractor (black color) is relatively large (compared with



**Figure 5.** Stability map in the  $(\eta-P)$  plane for (5a)  $\varepsilon = 0$  and (5b)  $\varepsilon = 0.011$ , with the same values of parameters as in Figure 1. The box below the figure (5a) is the magnification of the steady-state region.

Figure 5b) and the steady-state intensity region (green color) is small, as shown in Figure 5a. The box below the Figure (5a) represents the magnification of the stable locking state and periodic state regions. The Hopf bifurcation points (blue color) are seen as a boundary between the 2 states.

The regions of the periodic oscillation states are expanded over the gray regions and they also appear as narrow strips (or islands) embedded inside the chaotic region (marked by white).

We note that the dimension of the chaotic region is significantly affected by the gain saturation; for example, if we set  $\varepsilon = 0.011$  as a representative value (i.e. when the gain saturation effect is included), then the dynamical behavior of the laser system will considerably change, as shown in Figure 5b. The chaotic region is largely reduced compared to the one in Figure 5a and as a result the regions of the steady state and periodic state are expanded (stretched) and become wider, as shown in Figure 5b. The situation here clearly indicates the strong dependence of the features of dynamical behavior of the optically injected semiconductor laser system on the gain saturation coefficient ( $\varepsilon$ ). This suggests that  $\varepsilon$  is an effective control parameter in changing the dynamical characteristics of the semiconductor laser system and it needs to be included in the calculations of these characteristics in order to obtain more realistic results useful for practical applications.

#### 4. Conclusions

In this paper we have investigated the dynamical behavior and stability condition of the output intensity of an optically injected semiconductor laser with and without gain saturation effect. The rate equations model describing a semiconductor laser subjected to an optical injection are used in this investigation.

The variation in the dynamical behavior of the semiconductor laser system is achieved by varying the laser control parameters. We identify a route to chaos through different bifurcation transitions. This includes a sequence of period doubling, with small regions of P3 and P6 states, co-existence of periodic and chaotic oscillation states, and break up of different bifurcation branches. Furthermore, sudden transitions from periodic dynamics to chaos, as well as the reverse bifurcation process from chaotic to periodic dynamics and the transitions between the chaotic behaviors through the bifurcation process are observed. We have also examined the effect of changes in the phase of the laser field on the dynamical behavior of the laser system. We find that the laser phase parameter plays an important role in the dynamical behavior of the semiconductor laser system. In order to get a complete picture describing the different types of dynamical behavior of an optically injected semiconductor laser, we constructed 2 color stability maps, one including the effect of gain saturation and the other neglecting this effect. Different distinct regions of different dynamical behaviors are identified in these stability maps; their dimensions are significantly changed by changing the gain saturation coefficient ( $\varepsilon$ ).

The ability to control the dynamical behavior of optically injected semiconductor lasers simply by varying the values of the laser operating parameters in our investigations allows the possibility of choosing lasers with suitable parameters values. This laser can be used for different practical applications, such as photonic microwave, secure optical communications, and chaotic cryptography.

#### References

- [1] Wieszorek, S.; Simpson, T. B.; Krauskopf, B.; Lenstra, D. *Opt. Commun.* **2003**, *215*, 125–134.
- [2] Wieszorek, S.; Krauskopf, B.; Simpson, T.; Lenstra, D. *Phys. Rep.* **2005**, *416*, 1–128.
- [3] Ohtsubo, J. *Semiconductor Lasers: Stability, Instability, and Chaos*, 2nd ed.; Springer-Verlag: Berlin, Germany, 2007.
- [4] Chu, Y.-D.; Li, X.-F.; Zhang, J.-G.; Chang, Y.-X. *Chaos, Solitons & Fractals* **2009**, *41*, 14–27.

- [5] Erneux, T.; Glorieux, P. *Laser Dynamics*; Cambridge University Press: New York, NY, USA, 2010.
- [6] Perez, T.; Scire, A.; Van der Sande, G.; Colet, P.; Mirasso, C. R. *Opt. Express* **2007**, *15*, 12941–12948.
- [7] Tang S.; Liu, J. M. *Message Encoding / Decoding Using Chaotic Pulsing Semiconductor Lasers*, in *Optical Fiber Communication Conference and Exhibit, OFC 2001 Technical Digest Series*, Anaheim, vol. 3, paper WDD46, p. 46-1 to 46-3.
- [8] Mirasso, G. R. *SPIE, Newsroom*, **2010**, p. 1–3.
- [9] Hwang, S. K.; Chan, S. C.; Hsieh, S. C.; Li, C. Y. *Opt. Commun.* **2011**, *284*, 3581–3589.
- [10] Mirasso, C. R. *Applications of Semiconductor Lasers to Secure Communications*, in *Fundamental Issue of Nonlinear Laser Dynamics*, Krauskopf, B.; Lenstra, D., Eds.; *AIP Conference Proceeding* vol. 548, New York, USA, 2000, pp. 112–127.
- [11] Liu, J. M.; Chen, H. F.; Tang, S. *IEEE Quant. Electron.* **2002**, QE–38, 1184–1196.
- [12] Uchida, A.; Rogister, F.; Garcia-Ojalvo, J.; Roy, R. *Prog. Opt.* **2005**, *48*, 203–341.
- [13] Fundamental Issue of Nonlinear Laser Dynamics, Krauskopf, B.; Lenstra, D., Eds.; *AIP Conference Proceeding* vol. 548, New York, USA, 2000.
- [14] Parker, T. S.; Chua, L. S. *Practical Numerical Algorithms for Chaotic Systems*, Springer-Verlag: Berlin, Germany, 1989.
- [15] Lang, R.; Kobayashi, K. *IEEE J. Quant. Electron.* **1980**, QE–16, 347–355.
- [16] Simpson T. B.; Liu, M. *J. Appl. Phys.* **1993**, *73*, 2587–2589.
- [17] Gavrielides, A.; Kovanis, V.; Nizette, M.; Erneux, T.; Simpson, T. *J. Opt. B: Quant. Semiclass. Opt.* **2002**, *4*, 20–26.
- [18] Thomson, J. M.; Stewart, H. B. *Nonlinear Dynamics and Chaos*, Wiley: London, UK, 1986.